Journal of Materials Chemistry A

Accepted Manuscript

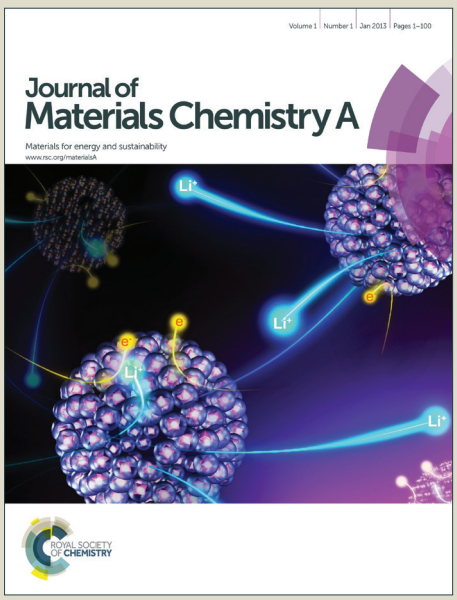

ROYAL SOCIETY OF CHEMISTRY

www.rsc.org/materialsA

One-step synthesis of Co-doped Zn_2SnO_4-graphene-carbon nanocomposites with improved lithium storage performances

Hui-Yuan Wang, Bang-Yong Wang, Jin-Kui Meng, Jin-Guo Wang* and Qi-Chuan Jiang*

Key Laboratory of Automobile Materials of Ministry of Education & School of Materials Science and Engineering, Nanling Campus, Jilin University, No. 5988 Renmin Street, Changchun 130025, PR China

Abstract: Co-doped Zn_2SnO_4-graphene-carbon nanocomposites have been prepared for the first time through a convenient one-step hydrothermal method. The size of Co-doped Zn_2SnO_4 nanoparticles is about 3-5 nm and they are well dispersed on graphene nanosheets and carbon layer. L-ascorbic acid is introduced to serve as reductant for GO and carbon sources. The doping of Co can enhance the crystalline degree of Zn_2SnO_4 nanoparticles. When evaluated as anode materials for lithium ion batteries, the Co-ZTO-G-C nanocomposites exhibit a significantly higher reversible capacity of 699 mAh g^{-1} after 50 cycles at 100 mA g^{-1} and an improved cycling stability with 461 mAh g^{-1} after 200 cycles at 500 mA g^{-1} compared with Co-ZTO-G and ZTO-G-C nanocomposites. Moreover, even at a high current density of 1000 mA g^{-1}, the reversible capacity of 418 mAh g^{-1} is still remained. The improved electrochemical performance can be attributed to the synergy of graphene substrate, the protective carbon layer, the uniform ultrafine Zn_2SnO_4 nanoparticles and Co doping. Therefore, Co-ZTO-G-C nanocomposites show great prospect as anode for lithium-ion batteries.

* Corresponding author: Professor Hui-Yuan Wang (H.-Y. Wang); Jin-Guo Wang (J.-G. Wang)
Tel/Fax: +86 431 8509 4699. E–mail: wanghuiyuan@jlu.edu.cn (H.-Y. Wang); jgwang@jlu.edu.cn (J.-G. Wang);

1. Introduction

Rechargeable lithium-ion batteries (LIBs) have been widely employed in small electronic devices, such as mobile phones, digital cameras, lap-top computers, owing to their superior energy density, cyclic life and environmental benignity since commercialization.[1-4] However, graphite could not meet the demand of consumers as commercial anodes because of its low theoretical capacity (372 mAh g^{-1}) and poor high-rate performance.[5] Therefore, searching for alternatives with excellent performance is greatly vital for the improvement of LIBs. Among available anode materials, tin-based materials have been regarded as very promising candidates because of their relatively high gravimetric capacity, natural abundance and intrinsically safety.[6-8] Since Idota et al.[9] firstly used amorphous tin oxides as a negative material in 1997, tin-based materials have become the research focuses and been studied extensively.

Recently, among tin-based materials, zinc stannate (Zn_2SnO_4) has attracted much attention due to its high electrical conductivity, its abundance, low cost and high theoretical capacity (1231 mAh g^{-1}).[10,11] In 2006, Rong et al.[10] synthesized Zn_2SnO_4 particles using hydrothermal methods, which for the first time were used as anode materials for LIBs and a reversible capacity of 580 mAh g^{-1} was maintained after 50 cycles at a current density of 100 mA g^{-1}. From then on, to improve the lithium storage of Zn_2SnO_4, different Zn_2SnO_4 nanostructures, such as cubes[12,15], boxes[13], nanowires[14] and nanoplates[14,15] have been investigated as anode materials. However, most of these materials mentioned above suffer from poor capacity as well as rapid capacity fading with the increase of cycling. The possible reason may arise from the huge volume changes during the alloying and dealloying processes of Li^+, resulting in their pulverization and exfoliation from current collector, which leads to capacity fading fast.[16] To solve these problems, one strategy is to design and fabricate active materials with various morphologies on the nanoscale. Nanostructured electrode materials are beneficial to increase the contact area of electrolyte and active materials and shorten the lithium ions diffusion distance.[14,17,18] Another strategy is to combine active materials with carbonaceous medium as a buffer layer, such as amorphous carbon and graphene. Carbonaceous medium can not only buffer the volume expansion of active materials during charge-discharge cycles, but also increase the electronic conductivity.[16,19,20] Song et al.[19] reported a

facile hydrothermal route for the synthesis of Zn_2SnO_4-nanocrystal/graphene-nanosheet nanohybrids. The Zn_2SnO_4/G hybrids exhibited an obvious improvement of electrochemical performance, and a charge capacity of 688 mAh g^{-1} was obtained after 50 cycles at 200 mA g^{-1}, while bare Zn_2SnO_4 only showed a charge capacity of 406 mAh g^{-1} after 50 cycles at 50 mA g^{-1}. Moreover, doping has also been confirmed to be an effective way to improve the electrochemical conductivity and charge transfer ability of electrode materials.[21,22]

In this work, we firstly report a one-step hydrothermal approach to fabricate a nanocomposite consisting of ultrafine Co-doped Zn_2SnO_4 nanoparticles, graphene nanosheets and amorphous carbon layers. Graphene has been regarded as a desirable substrate for metal oxide nanoparticles, due to its excellent electronic conductivity and mechanical flexibility. The coating of carbon layer can not only enhance the electronic conductivity of active materials, but also prevent the nanoparticles from peeling off from graphene sheet, resulting in an improvement in the cyclic stability and rate capacity of composite electrodes. Moreover, Co doping also can facilitate electronic conduction and lithium ion diffusion during the charging-discharging process. The morphologies, structures and electrochemical properties of the nanocomposites were investigated. Our results demonstrate that Co-doped Zn_2SnO_4-graphene-carbon nanocomposites exhibit a significantly enhanced cycle capacity and rate capability compared with those nanocomposites without amorphous carbon layer or Co doping.

2. Experimental Section

2.1 Material preparation

Analytical-grade $Zn(CH_3COO)_2{\cdot}2H_2O$, $Co(CH_3COO)_2{\cdot}4H_2O$, $Na_2SnO_3{\cdot}3H_2O$ and L-ascorbic acid were used as received without further purification. GO was prepared by the oxidation of natural flake graphite powder using a modified Hummers method.[23] In a typical procedure, 1.5 mmol $Zn(CH_3COO)_2{\cdot}2H_2O$ with 0.3 mmol $Co(CH_3COO)_2{\cdot}4H_2O$ and 1.5 mmol $Na_2SnO_3{\cdot}3H_2O$ were dissolved in 5 ml ethylene glycol with 15 ml of 1.8 mg ml^{-1} GO aqueous suspension, respectively. After that, the Na_2SnO_3 solution was poured into the $Zn(CH_3COO)_2$ solution under constant stirring for 10 min. Then the PH of the mixture was adjusted to about 9 with ammonia solution, followed by the

addition of 1 mmol L-ascorbic acid as reductant and carbon sources. The resulting mixture was stirred for 30 min and then transferred into a Teflon-lined stainless steel autoclave and heated to 180 ^{o}C for 12 h. After cooling to ambient temperature, the precipitate was collected by centrifuging and washing with DI water and ethanol, and freeze-dried in a vacuum environment. Finally, the products were calcined at 450 ^{o}C for 3 h under a N_2 atmosphere to get Co-doped Zn_2SnO_4-graphene-carbon nanocomposites (denoted as Co-ZTO-G-C nanocomposites). The composites prepared without adding NH_3 and L-ascorbic acid with the same procedure was named Co-ZTO-G nanocomposites and those prepared in the same route without the addition of $Co(CH_3COO)_2$ was named ZTO-G-C nanocomposites.

2.2 Material characterization

The crystal structures of the samples were characterized by powder X-ray diffraction (XRD, Rigaku-D/Max 2500PC/Japan, using Cu Kα radiation, λ = 1.5406 Å). The morphologies of the samples were investigated using field emission scanning electron microscopy (FESEM, JSM-6700F, Japan) and transmission electron microscopy (TEM, FEI-TECNAI G2 F20/America). Meanwhile, TEM elemental mapping were done using a Flash EA 1112 elemental analysis system (USA) equipped with energy dispersive X-ray spectroscopy (EDS, EDAX-Genesis/USA). Thermogravimetric analysis (TG, SDT-Q600, TA Instruments Inc. USA) was carried out under air flow (100 ml min^{-1}) over a temperature range of 20-800 ^{o}C at a heating rate of 10 ^{o}C min^{-1}. X-ray photo-electron spectrometry with an ESCALAB250 analyzer (XPS) were employed to evaluate the chemical status of the samples. The nitrogen adsorption and desorption isotherms were collected using ASAP 2020 surface area and porosity analyzer. The pore size distribution was calculated using the Barrett-Joyner-Halenda (BJH) methods.

2.3 Electrochemical measurements

The products were mixed with acetylene black and polyvinylidene fluoride which was resolved in N-methyl-2-pyrrolidone at a weight ratio of 70: 20: 10. The slurry was uniformly pasted on Cu foil. Such prepared electrode sheets were dried at 120 ^{o}C for 12 h in a vacuum oven. The CR2025-type half-coin cells were assembled in an argon-filled glove box with H_2O and O_2 contents below 1 ppm. Metallic lithium foil was used as the counter and reference electrode. The electrolyte consists of a solution of 1 M

$LiPF_6$ in a mixture of ethylene carbonate (EC), ethyl methyl carbonate (EMC) and dimethyl carbonate (DMC) with a volume ratio of 1: 1: 1. The typical mass loading in each electrode is ~1.0 mg cm^{-2}. Charge-discharge performance was evaluated by a LAND CT2001A battery instrument at a constant current density in the voltage range of 0.01-3.0 V at room temperature. The cyclic voltammetry (CV) test was performed between 0.01 and 3.0 V at a scan rate of 0.1 mV s^{-1} on a CHI650D electrochemical workstation. Electrochemical impedance spectra (EIS) was tested on the same instrument in the frequency range of 0.01 Hz-100 kHz at open circuit potential with an AC signal amplitude of 5 mV. Note that graphene itself can also contribute to the electrochemical capacities. Therefore, the specific capacities were calculated based on the nanocomposites.

3. Results and discussion

XPS spectra of Co-ZTO-G-C, Co-ZTO-G and ZTO-G-C nanocomposites were investigated, as shown in Fig. S1. The survey spectra show the three nanocomposites are mainly composed of Sn, Zn, O and C. The binding energies of Sn $3d_{3/2}$ and Sn $3d_{5/2}$ are found to be 494.66 eV and 485.89 eV, respectively. The peaks centered at 1020.31 eV and 1044.32 eV are assigned to the Zn $2p_{3/2}$ and Zn $2p_{1/2}$ peaks. Furthermore, two weak Co $2p_{3/2}$ and Co $2p_{1/2}$ peaks are observed at 780.84 eV and 796.61 eV for Co-ZTO-G-C nanocomposites with a spin-orbit splitting of about 15.77 eV (Fig. 1a), which are typical for Co in the oxidation state of Co^{2+}.[24-27] The C 1s spectra of the three composites exhibit four peaks corresponding to carbon atoms with different oxygenated functional groups, as shown in Fig. 1(b), (c) and (d). The location of the four peaks for C-C, C-O, C=O and O-C=O is at around 284.5 eV, 285.8 eV, 288 eV and 288.9 eV, respectively, for Co-ZTO-G-C nanocomposites. The peaks of the other two nanocomposites are almost the same as that of Co-ZTO-G-C nanocomposites. The intensity ratio of the four peaks for different composites was calculated, as shown in Table 1. Compared with Co-ZTO-G nanocomposites, Co-ZTO-G-C nanocomposites have higher content of C-C peaks and lower content of C-O peaks, which suggests that GO in Co-ZTO-G-C nanocomposites has been well reduced due to using L-ascorbic acid as reductant. However, the ratio of the oxygenated carbons to non-oxygenated carbons in ZTO-G-C nanocomposites is higher than that in Co-ZTO-G-C nanocomposites, which may

be because Co^{2+} doping into Zn_2SnO_4 nanoparticles strengthens the cation reaction with the oxygenated groups on the surface of GO, resulting in the removal of the oxygenated groups from its surface easily. However, the influence and detailed mechanism of Co^{2+} on the reduction of GO need further study.

X-ray diffraction patterns of the obtained Co-ZTO-G-C, Co-ZTO-G and ZTO-G-C nanocomposites are shown in Fig. 2a. The patterns of the three samples are very similar and all diffraction peaks can be well indexed to cubic Zn_2SnO_4 with a space group Fd3m (JCPDS NO. 24-1470). No signatures of other crystalline by-products such as cobalt oxides are observed, indicating Co^{2+} was successfully doped into Zn_2SnO_4 nanoparticles and may replace Zn^{2+} and dissolve in the lattice of Zn_2SnO_4 due to the very similar radius of Co^{2+} (0.074 nm) and Zn^{2+} (0.074 nm). Broader peaks in XRD pattern make it difficult to observe the obvious shift after the doping Co into Zn_2SnO_4 nanoparticles. Interestingly, the crystalline degree of Co-ZTO-G-C nanocomposites is apparently higher than that of the other two nanocomposites (Fig. 2a), indicating Co doping and carbonization process can strengthen the crystallinity of Zn_2SnO_4 nanoparticles. However, the crystallinity of as-prepared nanocomposites is less than that of Zn_2SnO_4 synthesized by Rong et al.[10] The broadened peaks in the three composites are a reflection of the formation of fine Zn_2SnO_4 nanocrystals. The weight ratio of carbon in the three nanocomposites is evaluated by thermal gravimetric analysis in air, as shown in Fig. 2b. The significant difference of the lost weight of Co-ZTO-G-C and Co-ZTO-G nanocomposites manifests L-ascorbic acid has been carbonized during hydrothermal process at 180 ^{o}C.[28] The lost weight of the three nanocomposites corresponds to the oxidation of graphene and amorphous carbon layer to CO_2 except for the evaporation of the absorbed water. According to the changed weight of the three composites, the weight percentage of carbon in Co-ZTO-G-C, Co-ZTO-G and ZTO-G-C nanocomposites is about 12.5%, 5.5% and 15%, respectively.

The morphologies and structures of the three nanocomposites were characterized by FESEM, as shown in Fig. S2. Obviously, graphene exhibits crumple morphology in Co-ZTO-G-C nanocomposites and is embedded in the other two nanocomposites. Detailed morphologies of Co-ZTO-G-C nanocomposites were further characterized by TEM (Fig. 3). Fig. 3a displays TEM image of Co-ZTO-

G-C nanocomposites under a low magnification, demonstrating thin paper-like graphene nanosheets. The magnified TEM image shows that the ultrafine Co-doped Zn_2SnO_4 nanocrystals are uniformly dispersed within graphene nanosheets (Fig. 3b). The corresponding selected area electron diffraction (SAED) pattern shows a series of diffraction rings which can be indexed to the (220), (311), (422) and (440) planes of cubic-structured Zn_2SnO_4 (the inset of Fig. 3b). The presence of diffraction rings in the SAED pattern indicates the polycrystalline nature of Zn_2SnO_4. The HRTEM image of the nanocomposites is shown in Fig. 3c. The lattice fringes with a spacing of 0.30 nm can be clearly observed, corresponding to the (220) plane of cubic-structured Zn_2SnO_4, which is consistent with the SAED analysis. The particle size distribution of Co-doped Zn_2SnO_4 nanoparticles was measured, as shown in Fig. 3d, and the average particle size is mainly within the range of 3-5 nm. Meanwhile, void spaces are also observed among the Zn_2SnO_4 nanoparticles, which was beneficial for electrolyte penetration during the electrochemical test. Scanning TEM (STEM) and elemental mapping analyses of Co-ZTO-G-C nanocomposites were carried out, as shown in Fig. 4a-f. It can be observed that Co element uniformly distributes in the nanocomposites (Fig. 4d). Meanwhile, based on the STEM area, the energy dispersive X-ray spectroscopy (EDX) analysis of Co-ZTO-G-C nanocomposites was also performed and summarized in Table S1. The atomic percentage of Co doping is estimated to be ~10 % for Co-ZTO-G-C nanocomposites.

The N_2 adsorption-desorption isotherms and the corresponding pore size distribution curves of Co-ZTO-G-C, Co-ZTO-G and ZTO-G-C nanocomposites are shown in Fig. S3. The three kinds of nanocomposites exhibit a typical type IV characteristic with an obvious capillary condensation step, indicating a mesoporous nature of the nanocomposites.[21,29] The BET specific surface areas of the three nanocomposites are measured to be about 144.5, 118.9 and 150.9 $m^2 g^{-1}$, respectively (Table S2). Co-ZTO-G nanocomposites exhibit lower specific surface areas than the other two nanocomposites due to the aggregation of graphene without the addition of NH_3 and L-ascorbic acid. It can also be found that Co-ZTO-G-C and ZTO-G-C nanocomposites possess nearly specific surface areas, indicating Co doping does not result in the change of surface areas obviously. It is well known that nanocomposites with large

surface areas are useful to increase the contact area of electrolyte/active materials and enhance the lithium storage performance.[30] Furthermore, The three nanocomposites have large pore volume and pore size, which will benefit electrolyte penetration, lithium ion diffusion and volume buffering during the lithiation and delithiation process.

To investigate the mechanism of reactions between Li^+ and active materials, the cyclic voltammetry test was carried out (Fig. 5a). Only two small peaks centred at 1.14 and 1.52 V are observed in the first cathodic scan of Co-ZTO-G-C nanocomposites, which disappeared in subsequent cycles. It may be attributed to a small amount of inserted lithium in the crystal structure of Zn_2SnO_4.[15,31,32] The appearance of the peaks is due to the small particle size.[15,31,32] In the second cycle the small cathodic peak is located around 0.12 V (vs Li^+/Li) and the main cathodic peak is located around 0.79 V, illustrating the different lithium reaction process. The redox couple indexed as 0.12/0.59 V corresponds to the alloying/dealloying process of Li_xSn and Li_yZn, while another redox couple indexed as 0.79/1.38 V originates from the partially reversible oxidation of Sn and Zn. Galvanostatic charge/discharge and cycling measurements were conducted at a current density of 100 mA g^{-1} in a voltage window of 0.01-3.0 V. As shown in Fig. 5b, Co-ZTO-G-C nanocomposites deliver a discharge capacity of 1260 mAh g^{-1} and a charge capacity of 786 mAh g^{-1} for the first cycle, corresponding to the initial coulombic efficiency of 62.3%. The capacity losses are considered inevitable due to the formation of a solid electrolyte interface (SEI) on the electrode surface. In the subsequent cycle, the coulombic efficiency rapidly increases to >94% and then is stable throughout the entire cycle tests.

The cycle performance of Co-ZTO-G-C, Co-ZTO-G and ZTO-G-C nanocomposites measured at 100 mA g^{-1} is shown in Fig. 5c. Compared with the other two nanocomposites, Co-ZTO-G-C nanocomposites exhibit a very stable cyclic performance. After 50 cycles, the reversible capacity of 699 mAh g^{-1} for Co-ZTO-G-C nanocomposites is still retained and about 86.9% of the corresponding initial capacity is maintained. Nevertheless, the capacities of Co-ZTO-G and ZTO-G-C nanocomposites exhibit a rapid decay with increasing cycles. After 50 cycles, the reversible capacities dramatically drop to 407 and 386 mAh g^{-1}, respectively and only about 49.4 and 59.8% of the corresponding initial

capacity is maintained. Furthermore, the rate capacities of the three nanocomposites were investigated at various rates from 100 to 1000 mA g^{-1} (Fig. 5d). Compared with the other two nanocomposites, Co-ZTO-G-C nanocomposites deliver higher lithium storage capacity at each current density. Even at a high current density of 1000 mA g^{-1}, high reversible capacity of 418 mAh g^{-1} is still remained. Moreover, a specific capacity of around 692 mAh g^{-1} is restored when the current density is reversed to 100 mA g^{-1}. The improvement in cyclic stability and rate capacity of Co-ZTO-G-C nanocomposites can be attributed to the amorphous carbon layer and Co doping. Firstly, the amorphous carbon layer coated on the surface of Zn_2SnO_4 nanoparticles and graphene nanosheets can prevent Zn_2SnO_4 nanoparticles from dropping off from graphene nanosheets, which is beneficial to increase the cyclic stability. Secondly, the carbon layer can make up a conducting network and increase the electronic conductivity. Thirdly, Co doping can facilitate electronic conduction and lithium ion diffusion, which contributes to the enhancement of the rate capacity.

To evaluate the long-term cyclic performance, the capacities of three nanocomposites were measured at 500 mA g^{-1}, as shown in Fig. 6. In the initial 2 cycles, the electrodes are firstly activated at a low current density of 100 mA g^{-1} and then undergo the subsequent cycles at 500 mA g^{-1}. Co-ZTO-G and ZTO-G-C nanocomposites show reversible capacities of 195 and 350 mAh g^{-1} after 200 cycles, respectively. In contrast, Co-ZTO-G-C nanocomposites deliver a capacity of 461 mAh g^{-1}, which is higher than the theoretical capacity of commercial graphite electrodes (372 mAh g^{-1}), indicating an improved rate capacity and cyclic stability of Co-ZTO-G-C nanocomposites. To further investigate the effects of carbon layer and Co doping in Co-ZTO-G-C nanocomposites, the three nanocomposites after 2 charge-discharge processes were investigated by electrochemical impedance spectroscopy (EIS) measurement (Fig. 7). All the impedance responses show a semicircular loop at high and medium frequency and a straight line at low frequency.[21] According to the previous works, the semicircle in medium-frequency region is assigned to the charge-transfer impedance on the electrode/electrolyte interface.[21,32,34] From the plots of the three nanocomposites, the semicircle of Co-ZTO-G-C nanocomposites is much smaller than that of the other two nanocomposites, corresponding to their lower

charge-transfer resistances. This can be further supported by simulating AC impedance spectra based on the modified Randles equivalent circuit (the inset of Fig. 7).[33,35,36] The fitted impedance parameters are listed in Table S3. The value of charge-transfer resistances (R_{ct}) of Co-ZTO-G-C nanocomposites is 47.4 Ω, which is significantly smaller than that of the other two nanocomposites (112.9 and 72.4 Ω). This result confirms that amorphous carbon layer and Co doping can facilitate Li^+ and electron transfer between electrolyte and Co-ZTO-G-C nanocomposites, which will result in the improvement of rate capacity and cyclic stability.

The outstanding electrochemical performance of Co-ZTO-G-C nanocomposites can be attributed to the synergistic effects of graphene nanosheets and carbon layer, as well as the doping of Co. The graphene nanosheets function as a substrate not only enhancing the conductivity of the composites but also accommodating volume expansion. Also, graphene could have the capability to disperse the nanoparticles during the synthesis process. The ultrafine Zn_2SnO_4 nanoparticles are advantageous because it can provide a large surface area and more activated sites for lithium storage. Introducing the carbon layer on the surface of the composites can keep the active materials affix on the graphene nanosheets and suppress the separation of Zn_2SnO_4 nanoparticles from the graphene substrate even at high rate after long cycles. Besides, it also plays additional functions as a stress buffer and an electronic conductor. Furthermore, the doping of Co can enhance the electronic conductivity and lithium ion diffusion, contributing to the improvement of rate capacity and cyclic stability.

4. Conclusions

In summary, Co-doped Zn_2SnO_4-graphene-carbon nanocomposites were firstly synthesized by a one-step hydrothermal method. The as-obtained nanocomposites reveal a uniform distribution of ultrafine Co-doped Zn_2SnO_4 nanoparticles 3-5 nm in size between graphene nanosheets and the carbon layer. The unique structure delivers a high reversible capacity of 699 mAh g^{-1} after 50 cycles at 100 mA g^{-1}, and a high rate capacity of 461 mAh g^{-1} after 200 cycles at 500 mA g^{-1}. The excellent electrochemical performance of Co-ZTO-G-C nanocomposites is attributed to the cooperation of graphene nanosheets and carbon layer, which effectively buffers the volume changes during lithium ion

intercalation/deintercalation process, enhances the electronic conductivity and prevents the detachment of Zn_2SnO_4 nanoparticles from graphene substrate. The doping of Co is another significant factor that further increases electron transport and lithium ion diffusion. Therefore, Co-ZTO-G-C nanocomposites hold great promise for the development of lithium ion batteries.

Acknowledgment

The authors acknowledge financial support from Foundation of Jilin University for Distinguished Young Scholars and Project 985-Materials Science and Engineering of Jilin University.

Supporting Information: Survey XPS spectra, FESEM images, N_2 adsorption-desorption isotherm loop and pore-size distribution plots and Kinetic parameters of Co-ZTO-G-C, Co-ZTO-G and ZTO-G-C nanocomposites.

References

1 P. G. Bruce, B. Scrosati and J. M. Tarascon, *Angew. Chem. Int. Ed.*, 2008, **47**, 2930.

2 Y. G. Guo, J. S. Hu and L. J. Wan, *Adv. Mater.*, 2008, **20**, 2878.

3 B. Kang and G. Ceder, *Nature*, 2009, **458**, 190.

4 Z. Chen, D. Q. Zhang, X. L. Wang, X. L. Jia, F. Wei, H. X. Li and Y. F. Lu, *Adv. Mater.*, 2012, **24**, 2030.

5 J. Cabana, L. Monconduit, D. Larcher and M. R. Palacín, *Adv. Mater.*, 2010, **22**, E170.

6 M. S. Park, Y. M. Kang, G. X. Wang, S. X. Dou and H. K. Liu, *Adv. Funct. Mater.*, 2008, **18**, 455.

7 R. D. Cakan, Y. S. Hu, M. Antonietti, J. Maier and M. M. Titirici, *Chem. Mater.*, 2008, **20**, 1227.

8 K. Shiva, S. Asokanb and A. J. Bhattacharyya, *Nanoscale*, 2011, **3**, 1501.

9 Y. Idota, T. Kubota, A. Matsufuji, Y. Maekawa, T. Miyasaka, *Science*, 1997, **276(5317)**, 1395.

10 A. Rong, X. P. Gao, G. R. Li, T. Y. Yan, H. Y. Zhu, J. Q. Qu and D. Y. Song, *J. Phys. Chem. B*, 2006, **110**, 14754.

11 J. Zeng, M. D. Xin, K. W Li, H. Wang, H. Yan and W. J. Zhang, *J. Phys. Chem. C*, 2008, **112**, 4159.

12 N.Feng, S. L. Peng, X. L. Sun, L. Qiao, X. W. Li, P. Wang, D. K. Hu and D. Y. He, *Materials Letters*, 2012, **76**, 66.

13 Y. Zhao, Y. Huang, Q. F. Wang, K. Wang, M. Zong, L. Wang, W. Zhang and X. Sun, *RSC Adv.*, 2013, **3**, 14480.

14 C. T. Cherian, M. R. Zheng, M. V. Reddy, B. V. R. Chowdari and C. H. Sow, *Appl. Mater. Interfaces*, 2013, **5**, 6054.

15 Y. J. Chen, B. H. Qu, L. Mei, D. N. Lei, L. B. Chen, Q. H. Li and T. H. Wang, *J. Mater. Chem.*, 2012, **22**, 25373.

16 X. Z. Zheng, Y. F. Li, Y. X. Xu, Z. S. Hong and M. D. Wei, *CrystEngComm.*, 2012, **14**, 2112.

17 Y. Chen, B. H. Song, R. M. Chen, L. Lu and J. M. Xue, *J. Mater. Chem. A*, 2014, **2**, 5688.

18 W. Fu, F. H. Du, K. X. Wang, T. N. Ye, X. Wei and J. S. Chen, *J. Mater. Chem. A*, 2014, **2**, 6960.

19 W. T. Song, J. Xie, W. Y. Hu, S. Y. Liu, G. S. Cao, T. J. Zhu and X. B. Zhao, *Journal of Power Sources*, 2013, **229**, 6.

20 Y. Zhao, Y. Huang, W. Zhang, Q. F. Wang, K. Wang, M. Zong and X. Sun, *RSC Adv.*, 2013, **3**, 23489.

21 Q. Li, L. W. Yin, Z. Q. Li, X. K. Wang, Y. X. Qi and J. Y. Ma, *Appl. Mater. Interfaces*, 2013, **5**, 10975.

22 Z. Ali, S. N. Cha, J. I. Sohn, I. Shakir, C. Yan, J. M. Kim and D. J. Kang, J. Mater. Chem., 2012, 22, 17625.

23 D. C. Marcano, D. V. Kosynkin, J. M. Berlin, A. Sinitskii, Z. Z. Sun, A. Slesarev, L. B. Alemany, W. Lu and J. M. Tour, *ACS NANO*, 2010, **4**, 4806.

24 J. R. Huang, L. Y. Wang, C. P. Gu, M. H. Zhai and J. H. Liu, *CrystEngComm.*, 2013, **15**, 7515.

25 Y. F. Wang, K. N. Li,Y. F. Xu, C. Y. Su and D. B. Kuang, *Nano Energy*, 2013, **2**, 1287.

26 Y. J. Mai, J. P. Tu, X. H. Xia, C. D. Gu and X. L. Wang, *Journal of Power Sources*, 2011, **196**,

6388.

27 J. F. Li, S. L. Xiong, X. W. Lia and Y. T. Qian, *J. Mater. Chem.*, 2012, **22**, 23254.

28 B. Ellis, W. H. Kan, W. R. M. Makahnouk and L. F. Nazar, *J. Mater. Chem.*, 2007, **17**, 3248.

29 G. Y. Liu, H. Y. Wang, G. Q. Liu, Z. Z. Yang, B. Jin and Q. C. Jiang, *Electrochimica Acta*, 2013, **87**, 218.

30 B. B. Chen, H. Qian, J. H. Xu, L. L. Qin, Q. H. Wu, M. S. Zheng and Q. F. Dong, *J. Mater. Chem. A*, 2014, **2**, 9345.

31 F. Han, W. C. Li, C. Lei, B. He, K. Oshida and A. H. Lu, *small*, 2014, DOI: 10.1002/smll.201400371.

32 B. Sun, J. Horvat, H. S. Kim, W. S. Kim, J. Ahn and G. Wang, *J. Phys. Chem. C*, 2010, **114**, 18753.

33 W. Zhang, W. D. Zhou, J. H. Wright, Y. N. Kim, D. W. Liu and X. C. Xiao, *Appl. Mater. Interfaces*, 2014, **6**, 7292.

34 Y. L. Xiao, J. T. Zai, X. M. Li, Y. Gong, B. Li, Q. Y. Han and X. F. Qian, *Nano Energy*, 2014, **6**, 51.

35 S. B. Yang , X. L. Feng and K. Müllen, *Adv. Mater.*, 2011, **23**, 3575.

36 L. T. Anh, A. K. Rai, T. V. Thi, J. Gim, S. Kim,V. Mathew and Jaekook Kim, *J. Mater. Chem. A*, 2014, **2**, 6966.

Figure captions:

Figure 1. High resolution XPS spectra of (a) Co 2p of Co-ZTO-G-C nanocomposites, C 1s of (b) Co-ZTO-G-C, (c) Co-ZTO-G and (d) ZTO-G-C nanocomposites.

Figure 2. (a) XRD patterns and (b) TG analyses of Co-ZTO-G-C, Co-ZTO-G and ZTO-G-C nanocomposites.

Figure 3. (a) and (b) TEM images of Co-ZTO-G-C nanocomposites. Inset of (b): corresponding SAED pattern. (c) High-resolution TEM image and (d) particle size distribution.

Figure 4. (a) STEM image of Co-ZTO-G-C nanocomposites and (b-f) corresponding elemental mapping images of Zn, Sn, Co, O and C.

Figure 5. (a) Cyclic voltammetry curves of Co-ZTO-G-C nanocomposites in the voltage window of 0.01-3.0 V at a scan rate of 0.1 mV s^{-1}, (b) charge/discharge profiles of Co-ZTO-G-C nanocomposites at 100 mA g^{-1}, (c) cyclic performance of Co-ZTO-G-C, Co-ZTO-G and ZTO-G-C nanocomposites at 100 mA g^{-1}, (d) rate performance of three nanocomposites at current densities in the range of 100-1000 mA g^{-1}.

Figure 6. Cycle performance of Co-ZTO-G-C, Co-ZTO-G and ZTO-G-C nanocomposites at 500 mAg^{-1}.

Figure 7. AC impedance spectra of Co-ZTO-G-C, Co-ZTO-G and ZTO-G-C nanocomposites and equivalent circuit model (inset).

Table captions:

Table 1 Intensity ratios of C-C, C-O, C=O and O-C=O for different nanocomposites.

Figure 1

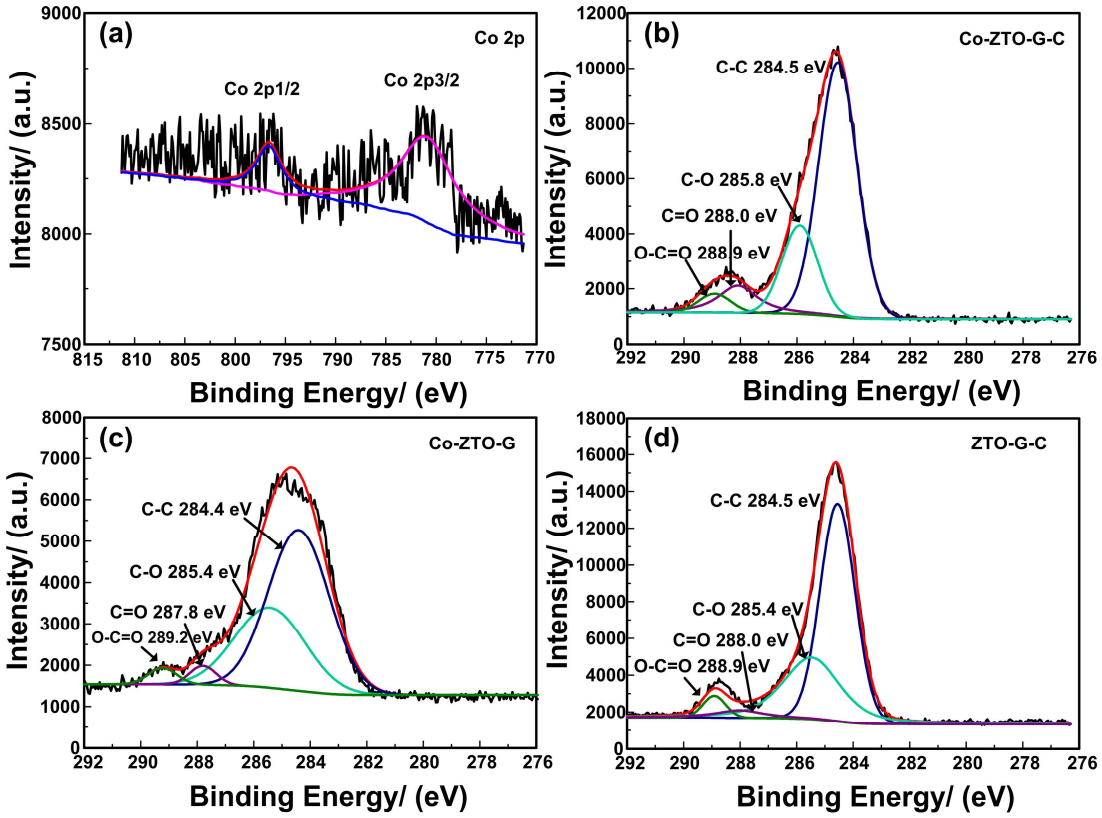

Table 1

Composites	C-C (%)	C-O (%)	C=O (%)	O-C=O (%)
Co-ZTO-G-C	65.4	20.9	9.7	4.0
Co-ZTO-G	59.8	34.3	3.0	2.8
ZTO-G-C	58.9	33.0	4.1	3.9

Figure 2

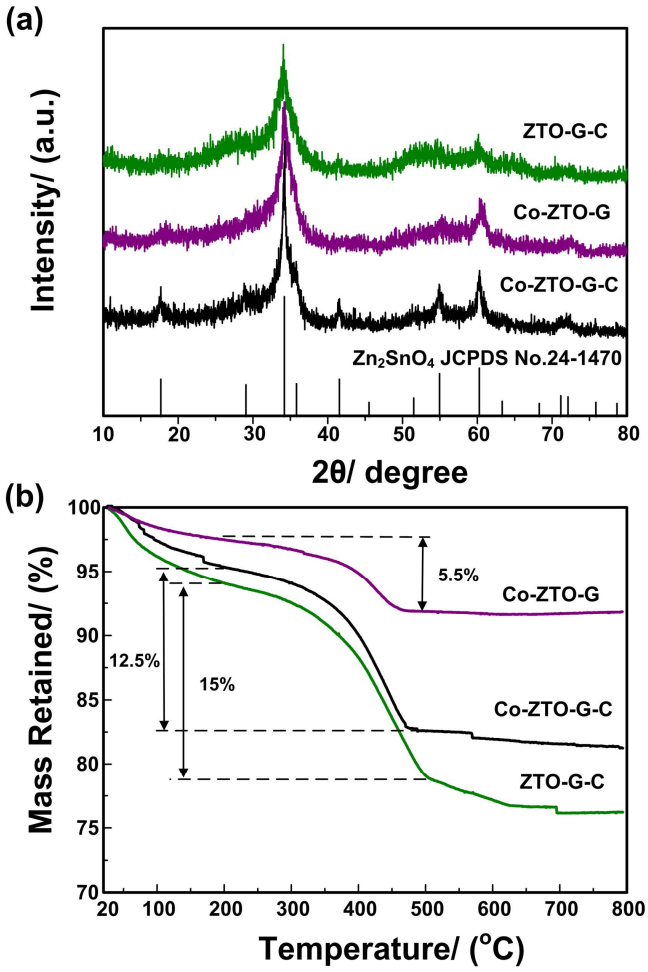

Figure 3

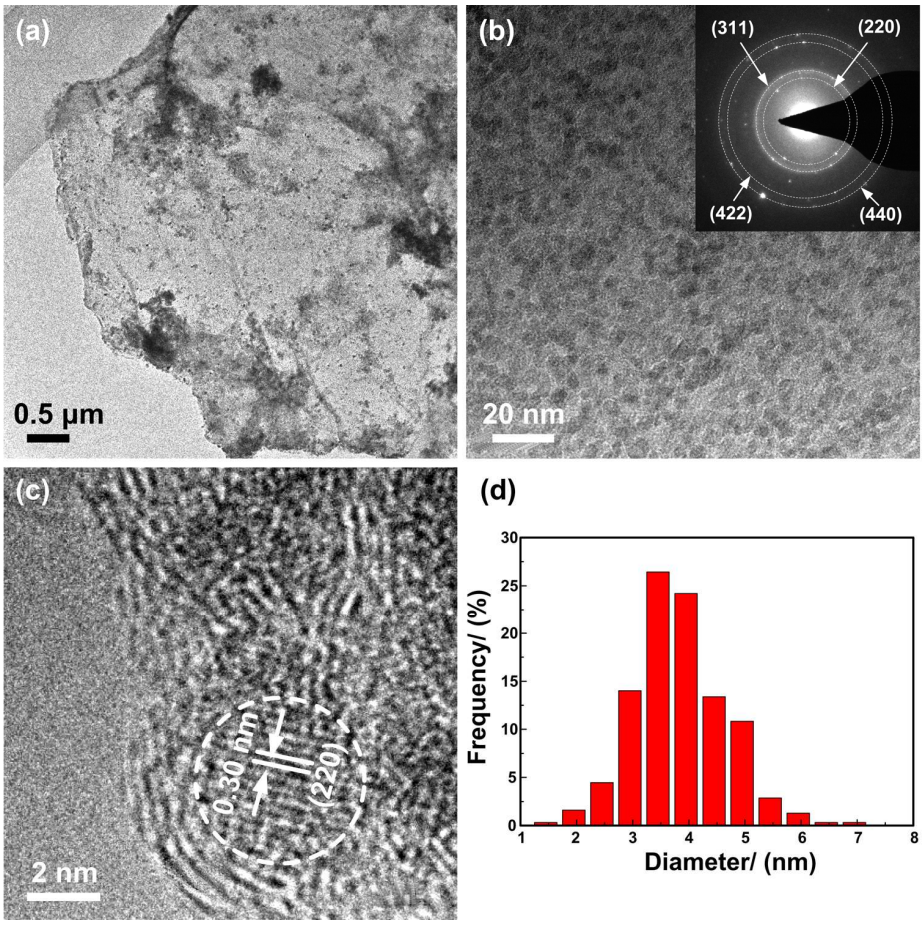

Figure 4

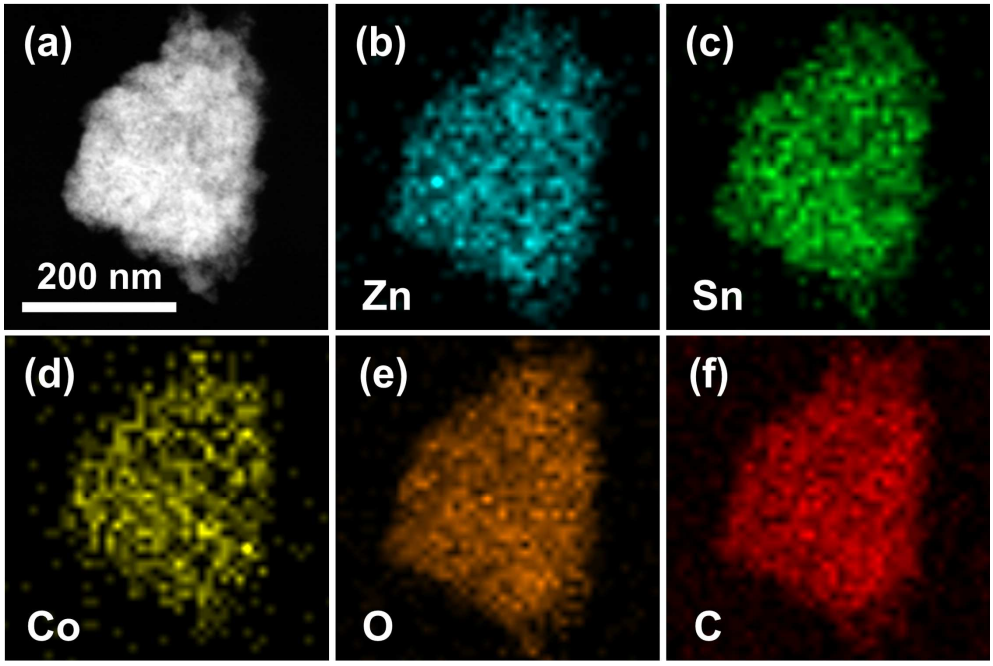

Figure 5

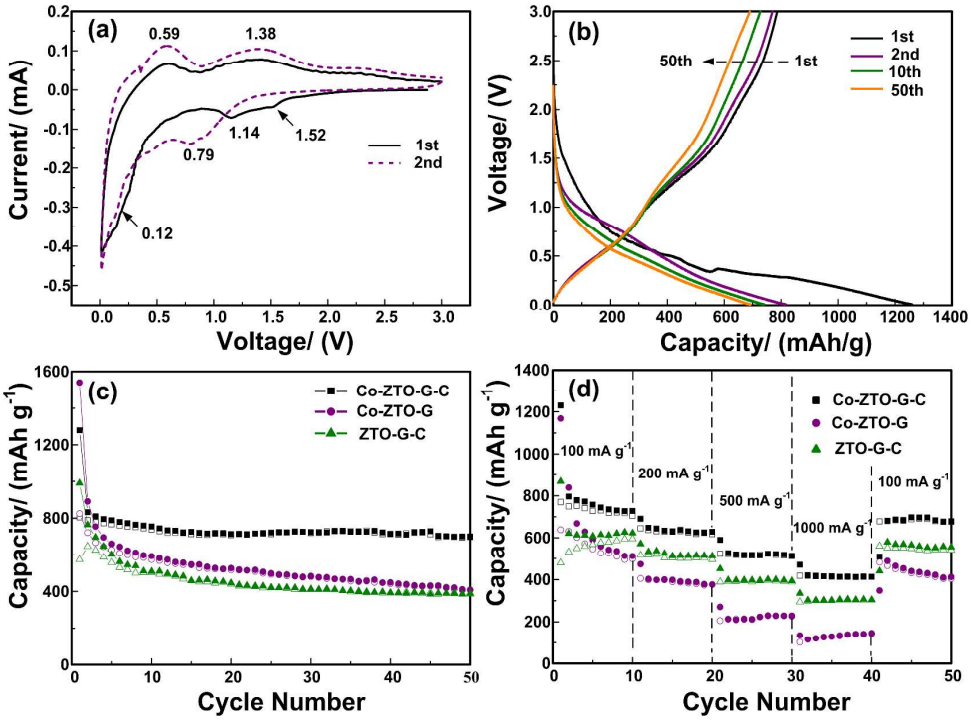

Figure 6

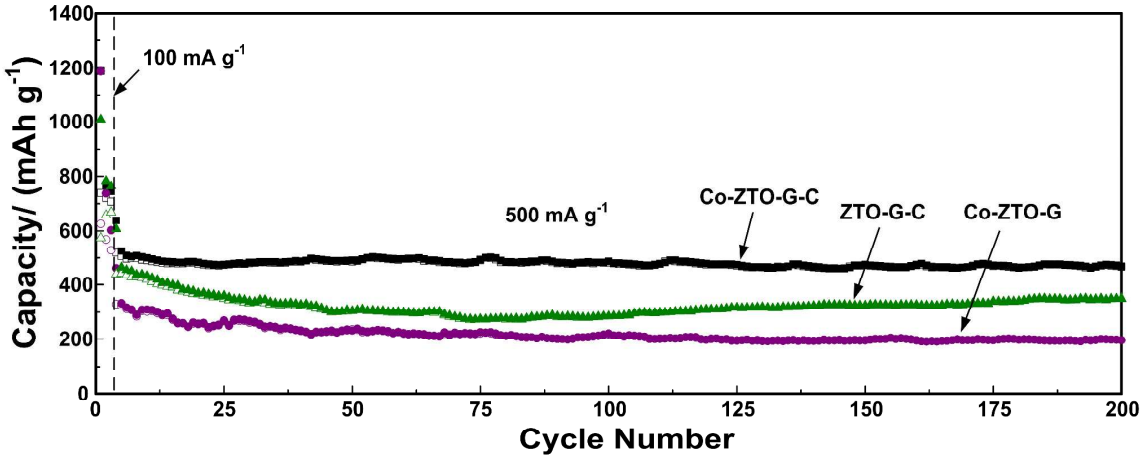

Figure 7